Cellular and Molecular Life Sciences (2022) 79:407
https://doi.org/10.1007/s00018-022-04441-9

ORIGINAL ARTICLE

Adtrp regulates thermogenic activity of adipose tissue via mediating the secretion of S100b

Peng Li[1] · Runjie Song[1] · Yaqi Du[1] · Huijiao Liu[1] · Xiangdong Li[1,2,3]

Received: 15 December 2021 / Revised: 14 June 2022 / Accepted: 19 June 2022 / Published online: 8 July 2022

Abstract

Brown and beige adipose tissues dissipate chemical energy in the form of heat to maintain your body temperature in cold conditions. The impaired function of these tissues results in various metabolic diseases in humans and mice. By bioinformatical analyses, we identified a functional thermogenic regulator of adipose tissue, *Androgen-dependent tissue factor pathway inhibitor [TFPI]-regulating protein* (*Adtrp*), which was significantly overexpressed in and functionally activated the mature brown/beige adipocytes. Hereby, we knocked out *Adtrp* in mice which led to multiple abnormalities in thermogenesis, metabolism, and maturation of brown/beige adipocytes causing excess lipid accumulation in brown adipose tissue (BAT) and cold intolerance. The capability of thermogenesis in brown/beige adipose tissues could be recovered in *Adtrp* KO mice upon direct β3-adrenergic receptor (β3-AR) stimulation by CL316,243 treatment. Our mechanistic studies revealed that Adtrp by binding to S100 calcium-binding protein b (S100b) indirectly mediated the secretion of S100b, which in turn promoted the β3-AR mediated thermogenesis via sympathetic innervation. These results may provide a novel insight into *Adtrp* in metabolism via regulating the differentiation and thermogenesis of adipose tissues in mice.

Keywords *Adtrp* · BAT · iWAT · Thermogenesis · Differentiation · S100b

Abbreviations

Adtrp	*Androgen-dependent tissue factor pathway inhibitor (TFPI)-regulating protein*
BAT	Brown adipose tissue
β3-AR	β-Adrenergic receptor
S100b	*S100 calcium-binding protein b*
WAT	White adipose tissue
Ucp1	*Uncoupling protein-1*
SNS	Sympathetic nervous system
CAD	Coronary artery disease
ECs	Endothelial cells
FAHFAs	Fatty acid esters of hydroxy fatty acids
iWAT	Inguinal WAT
eWAT	Epididymis WAT
GEO	Gene Expression Omnibus
KO	Knockout
SVF	Stromal vascular fraction
CRISPR/Cas9	Clustered regularly interspaced short palindromic repeats/CRISPR associated 9
SFP	Specific pathogen-free
DEGs	Differentially expressed genes
hTERT	Human telomerase reverse transcriptase
DMEM	Dulbecco's modified Eagle's medium
FBS	Fetal bovine serum
TG	Triglyceride
FFA	Free fatty acid
RT-PCR	Reverse transcription PCR
RT-qPCR	Quantitative reverse transcription PCR
M-MLV	Moloney Murine Leukemia Virus
Fabp4	*Fatty acid-binding protein 4*
Dio2	*Deiodinase, iodothyronine, type II*
Cidea	*Cell death-inducing DFFA-like effector A*
Cox8b	*Cytochrome c oxidase subunit 8b*
Pgc1α	*Peroxisome proliferative activated receptor, gamma, coactivator 1 alpha*
Pparγ	*Peroxisome proliferator-activated receptor gamma*

Peng Li, Runjie Song and Yaqi Du contributed equally to this work.

✉ Xiangdong Li
xiangdongli68@126.com

[1] State Key Laboratory of Agrobiotechnology, College of Biological Sciences, China Agricultural University, Beijing 100193, China

[2] Department of Reproduction and Gynecological Endocrinology, Medical University of Bialystok, Białystok, Poland

[3] Department of Nutrition and Health, China Agricultural University, Beijing 100193, China

Prdm16	*PR domain containing 16*
GTT	Glucose Tolerance Test
ITT	Insulin Tolerance Test
VCO_2	Carbon dioxide generation
VO_2	Oxygen consumption
EE	Energy expenditure
OCR	Oxygen Consumption Rate
ECAR	Extracellular Acidification Rate
FCCP	Carbonyl cyanide-4-(trifluoromethoxy) phenylhydrazone
AA	Antimycin A
Rot	Rotenone
2-DG	2-Deoxy-D-glucose
BCA	Bicinchoninic acid
HE	Hematoxylin and Eosin
IHC	Immunohistochemistry
IF	Immunofluorescence
HRP	Horseradish Peroxidase
DAB	3,3′-Diaminobenzidine tetra-hydrochloride
FITC	Fluorescein isothiocyanate
Creb3	*cAMP-responsive element-binding protein 3*
IP	Immunoprecipitation
SDS-PAGE	Sodium Dodecyl Sulfate–Polyacrylamide Gel Electrophoresis
PVDF	Polyvinylidene fluoride
ECL	Enhanced chemiluminescence
Hsp90	*Heat shock protein 90*
hMSCs	Human mesenchymal stromal cells
ADIPOQ	*Adiponectin C1Q and collagen domain containing*
Gys2	*Glycogen synthase 2*
Elovl3	*Elongase of very long chain fatty acids-3*
AUC	Area Under Curve
CMTM7	*MARVEL transmembrane domain containing 7*
TMED8	*Transmembrane p24 trafficking protein family member 8*
VTN	*Vitronectin*
Clstn3β	*Calsyntenin 3β*
BM-MSC	Bone marrow MSC
HFD	High-fat diet
ERRγ	*Estrogen-related receptor gamma*
SNP	Single-nucleotide polymorphism

Introduction

Adipose tissues play critical roles in controlling the energy balance and metabolism, which makes them natural therapeutic targets to deal with obesity and metabolically disordered diseases [1, 2]. Adipose tissues are composed of brown adipose tissue (BAT) and white adipose tissue (WAT). Brown adipocytes are muscle-like cell lineages with multiple small lipid droplets and with abundant mitochondria [3, 4]. BAT highly expresses uncoupling protein-1 (UCP1) to uncouple respiration for thermogenesis in cold environments [5, 6]. Small mammals, especially rodents, have copious BAT and recent studies have shown that BAT existed in the neck and supraclavicular regions of adult human [7–9]. White adipocytes have large lipid droplets and their main function is to store excess energy [4]. However, in response to various stimuli, such as cold exposure or activator of the β3 adrenergic receptor (β3-AR), WAT can express UCP-1 for thermogenesis and UCP1-expressing WAT is called as beige adipocytes [10–12]. The sympathetic nervous system (SNS) controls the activation and thermogenesis of brown or beige adipocytes [13]. Upon cold exposure, SNS-released catecholamine or noradrenaline binds the β3-AR and activates its downstream pathways to dissipate energy as heat in adipose tissues [14–16].

Androgen-dependent tissue factor pathway inhibitor [TFPI]-regulating protein (*ADTRP*), also known as *C6ORF105*, has been reported as a coronary artery disease (CAD) susceptibility gene in human [17]. The deficiency of *ADTRP* also causes oral cleft syndrome and craniosynostosis in human [18, 19]. Functional studies have shown that androgens may induce ADTRP, and increased ADTRP could regulate the anticoagulant protection in endothelial cells (ECs) in vitro and vascular development, integrity and stability in vivo [20, 21]. ADTRP is further identified as an atypical hydrolytic enzyme to specifically hydrolyze fatty acid esters of hydroxy fatty acids (FAHFAs), a new class of bioactive lipids shown in vitro or in vivo [22–24].

Adtrp is highly expressed in liver, BAT, inguinal WAT (iWAT), epididymis WAT (eWAT), kidney and duodenum in mice [23]. *Adtrp* has been shown to participate in the regulatory functions of liver and adipose tissues [23], although a recent study has reported that *Adtrp* did not regulate the lipid and glucose metabolism in liver of mice [25]. However, the underlying functions and molecular mechanisms of *Adtrp* in adipose tissues are unknown.

Here, we hypothesized that *Adtrp* might play a crucial role in metabolism and thermogenesis of BAT and iWAT in mice. To test our hypothesis, we generated an *Adtrp* knockout (KO) mouse model to prove that *Adtrp* would drive the differentiation of BAT and iWAT stromal vascular fraction (SVF) cells and participate in the metabolism and thermogenesis of BAT and beige iWAT in vitro and in vivo. Additionally, we did mechanistic studies to show whether Adtrp was involved in the secretion of S100 calcium-binding protein b (S100b) to regulate the metabolic homeostasis and thermogenesis in mice.

Materials and methods

Animals

The *Adtrp* KO mouse model was generated by Nanjing biomedical research institute of Nanjing University via Clustered regularly interspaced short palindromic repeats/CRISPR associated 9 (CRISPR/Cas9) technology. Genotyping primers are listed in Table S1. 6-week-old male C57BL/6 J mice were purchased from the Si Pei Fu (SPF biotechnology Co., Ltd. China). Mice were housed under specific pathogen-free (SFP) conditions at 25 °C. All the studies were conducted with 8-week-old male mice with chow diet. For acute cold exposure, mouse was individually caged at 4 °C for 8 h, and the core body temperature of WT or *Adtrp* KO mice were measured every 2 h with a portable intelligent digital thermometer (CCCC Jianyi Technology Development Co., Ltd. China). The thermal images were captured by a thermal camera (FLIR, USA) at 4 °C. For a long-term 4 °C treatment, WT mouse was individually caged at 4 °C for 7 days, and WT mouse individually caged at 25 °C was used as control. For a long-term 16 °C treatment, WT or *Adtrp* KO mice were individually caged at 16 °C for 7 days. For β3-AR agonist treatment, mice were intraperitoneally injected with 1 mg/Kg CL316,243 (Sigma-Aldrich, USA), every day for 7 days, whereas intraperitoneal injection of 0.9% NaCl solution was used as control. All animals were sacrificed by inhalation of carbon dioxide.

Bioinformatics analysis

Gene microarray data of GSE13432 were re-analyzed by the limma package for biological statistics. RNA-seq data were acquired from the GSE86338, GSE104285, GSE129083, where edgeR or DESeq2 package was used for analysis of differentially expressed genes. The threshold of the differentially expressed genes (DEGs) in GSE86338, GSE104285, GSE13432 and GSE129083 was set as $\log_2$ fold change > 0.5 or $\log_2$ fold change < -0.5, p value < 0.05. All up-regulated genes are listed in the Supplementary Table S2–S6. Heatmaps for differential genes were analyzed by pheatmap package of R.

Cell culture

Human embryonic kidney cells (HEK) 293T (293T) cell line was purchased from the Cell Bank of the Peking Union Medical College Hospital (China. Licensed by ATCC). The human telomerase reverse transcriptase (hTERT) immortalized cell lines—hTERT A41hBAT-SVF and hTERT A41hWAT-SVF were purchased from American Type Culture Collection (ATCC, USA). Primary BAT SVF cells were isolated from the BAT of the newborn male mice and primary iWAT SVF cells were isolated from the iWAT of 4-week-old male mice as described previously [25–27]. Isolated adipose tissues were digested with 1.5 mg/mL type I collagenase (Sigma-Aldrich) at 37 °C for 40 min. After filtering and centrifuging, BAT and iWAT SVF cells were plated in the culture medium. Cells were cultured in Dulbecco's modified Eagle's medium (DMEM, Gibco, USA) with 10% fetal bovine serum (FBS, Gibco) at 37 °C with 5% CO_2. For differentiation of the primary adipocytes, cells were treated with the induction medium [DMEM with 10% FBS, 20 nM Insulin (Sigma-Aldrich), 1 nM T3 (Sigma-Aldrich), 0.5 mM Isobutylmethylxanthine (Sigma-Aldrich), 2 μg/mL Dexamethasone (Sigma-Aldrich), 1 μM Rosiglitazone (Sigma-Aldrich) and 125 nM Indomethacin (Sigma-Aldrich)] for 2 days and then the medium was replaced with the maintenance medium (DMEM with 10% FBS, 20 nM Insulin and 1 nM T3) for connective 4 days.

Serum analyses

Blood samples were collected by cardiac puncture after anesthesia by isoflurane inhalation. Serum was obtained from the blood samples after centrifuging at 3000 RPM for 5 min. Serum triglyceride (TG) determination kit (Sigma-Aldrich) and serum-free fatty acid (FFA) assay kit (Abcam, UK) were used to measure the serum TG and FFA of mice, separately.

RNA extraction, reverse transcription PCR (RT-PCR) and quantitative reverse transcription PCR (RT-qPCR)

Trizol reagent (Invitrogen, USA) was used to extract the total RNA from tissues and cells based on the manufacturer's instructions. Moloney Murine Leukemia Virus (M-MLV) Reverse Transcriptase (Takara, Japan) was used to synthesize cDNAs from the total RNA according to the manufacturer's instructions. RT-qPCR was performed using SYBR Green PCR Master Mix (Invitrogen) with the StepOnePlus System (Invitrogen) according to manufacturer's instructions. For analyzing the gene expressions of hTERT A41hBAT-SVF cells and hTERT A41hWAT-SVF cells, *β-ACTIN* was used as the house keeping internal control gene to normalize *ADTRP*; *UCP1*; *Fatty Acid-Binding Protein 4* (*FABP4*). For analyzing the gene expressions of mice samples, *β-Actin* was used as the internal control to normalize *Adtrp*; *Ucp1; Deiodinase, iodothyronine, type II* (*Dio2*); *Cell death-inducing DFFA-like effector A (Cidea); Cytochrome c oxidase subunit 8b (Cox8b); Peroxisome*

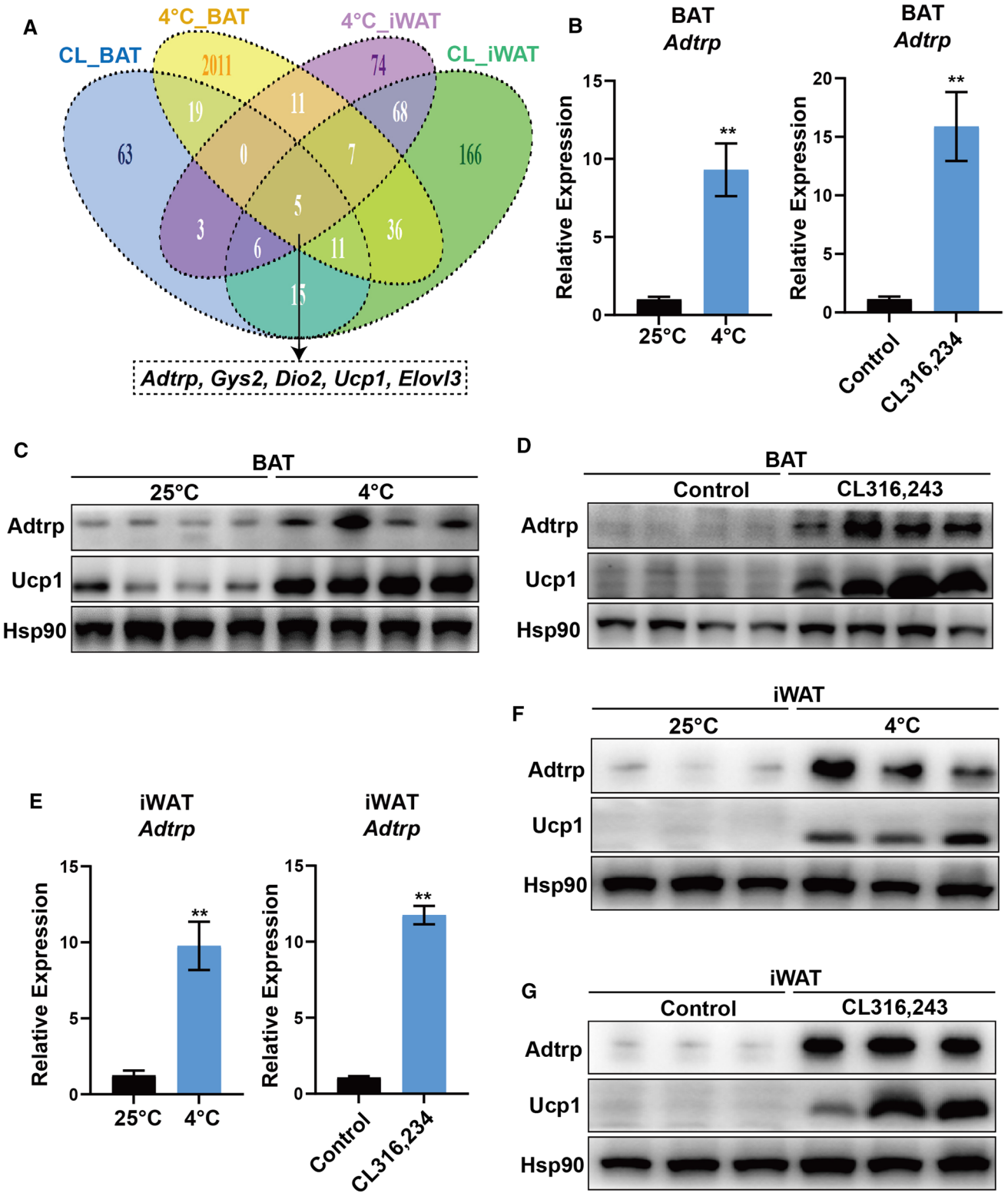
A
4°C_BAT
4°C_iWAT
CL_BAT
CL_iWAT
2011
74
19
11
68
63
0
7
166
5
3
6
36
11
15
Adtrp, Gys2, Dio2, Ucp1, Elovl3
B
BAT
Adtrp
Relative Expression
25°C
4°C
Control
CL316,234
C
BAT
25°C
4°C
Adtrp
Ucp1
Hsp90
D
BAT
Control
CL316,243
E
iWAT
Adtrp
F
iWAT
G

◂**Fig. 1** Effects of cold exposure or CL316,243 treatment on Adtrp expression in mice BAT and iWAT. **A** Schematic illustration showing genes expression profile at 4 °C or with CL316,243 treatment of mice BAT and iWAT predicted by overlapping GEO: GSE86338, GSE104285, GSE13432 and GSE129083 data. **B** RT-qPCR analysis of *Adtrp* in mice BAT with 4 °C treatment for 7 days ($n=5$) (25 °C treated mice as control) or CL316,243 injection for 7 days ($n=5$) (mice with the injection of 0.9% NaCl solution as control). **C** and **D** Western blot analyses of Adtrp and Ucp1 in mice BAT with 4 °C or CL316,243 treatment for 7 days, Hsp90 as the internal control ($n=4$). **E** RT-qPCR analysis of *Adtrp* in mice iWAT with 4 °C or CL316,243 treatment for 7 days ($n=5$). **F** and **G** Western blot analyses of Adtrp and Ucp1 in mice iWAT with 4 °C or CL316,243 treatment for 7 days, Hsp90 as the internal control ($n=3$). Error bars represent the means ± SEM of three independent experiments, $^{**}p<0.01$

proliferative activated receptor, gamma, coactivator 1 alpha (Pgc1α), Peroxisome proliferator-activated receptor gamma (Pparγ); Fabp4; PR domain containing 16 (Prdm16) and S100b. The relative expressions of these genes were calculated by $2^{-\Delta\Delta Ct}$ method. Primers are listed in Table S1.

Glucose Tolerance Test (GTT) and Insulin Tolerance Test (ITT)

For the GTT assay, 8-week-old male mice were fasted for 16 h and the glucose concentrations from the tail vein blood were measured by a glucometer (Roche, Switzerland) at 0, 15, 30, 45, 60, 90, 120 min after intraperitoneal injections with glucose (Sigma-Aldrich) (2 g/kg body weight). Two weeks later, an ITT assay was conducted with the same mice. Mice were fasted for 6 h and the glucose concentrations from the tail vein blood were measured at 0, 15, 30, 60, 90 min after intraperitoneally injecting with the insulin (Sigma-Aldrich) (0.75 U/kg body weight).

Indirect calorimetry

Mouse was individually caged and maintained with a 12 h light (07:00–19:00) and 12 h dark (19:00–07:00) cycle under 25 °C or 16 °C. Food and water intake, carbon dioxide (VCO_2) generation, oxygen consumption (VO_2) and calorimetry were measured by the Oxylet System (PANLAB, Spain) and total energy expenditure (EE) was calculated by the VO_2 and the resting energy requirements. The data were collected and analyzed by the METABOLISM 3.0 software (PANLAB).

Cellular metabolism assay

The mice BAT and iWAT SVF cells were plated and differentiated for 6 days on the Seahorse 24-well microplates (Agilent, USA). The oxygen consumption rate (OCR) and extracellular acidification rate (ECAR) of the cells were measured using a Seahorse XFe24 Analyzer (Agilent) according to the manufacturer's protocol and as per earlier publications [28, 29]. For the mitochondrial stress test, cells were treated with 25 mM glucose (Sigma-Aldrich), 1 mM pyruvate (Sigma-Aldrich) and 2 mM L-glutamine (Sigma-Aldrich) contained Seahorse XF Base Medium (Agilent) for 1 h at 37 °C without CO_2, and then measured with 3 times assay cycles for baseline and every treatment, including the injections with following order, 1.5 μM Oligomycin (Agilent), 1 μM Carbonyl cyanide-4-(trifluoromethoxy) phenylhydrazone (FCCP, Agilent), 0.5 μM of Antimycin A (AA, Agilent) and 0.5 μM Rotenone (Rot, Agilent), respectively, with the programs of (mixing for 3 min, waiting for 2 min and measurement lasting for 3 min). For the glycolysis stress test, cells were treated with 1 mM L-glutamine (Sigma-Aldrich) contained Seahorse XF Base Medium (Agilent) for 1 h at 37 °C without CO_2, and then cells were measured with 3 times assay cycles for baseline and every treatment, including the injections with following order, 10 mM Glucose (Agilent), 1 μM Oligomycin (Agilent), and 50 mM 2-Deoxy-D-glucose (2-DG, Agilent) respectively, with the programs of (mixing for 3 min, waiting for 2 min and measurement lasting for 3 min). After these assays, the total cell proteins/each well were extracted and quantified with a Bicinchoninic acid (BCA) protein quantification kit (Thermo Scientific, USA) for normalization. Seahorse Wave Desktop Software (Agilent) was used to analyze the results.

Hematoxylin and Eosin (HE), Immunohistochemistry (IHC) and Immunofluorescence (IF) analyses

The tissues were fixed with 4% paraformaldehyde, embedded in paraffin, and sectioned at 4 μm. After dewaxing, sections were stained with an HE staining kit (Solarbio, China) according to the manufacturer's instructions. For IHC and IF, sections were pretreated with hydrogen peroxide (3%) for 10 min to remove the endogenous peroxidase, followed by antigen retrieval in a microwave for 15 min in 10 mM citrate buffer (pH 6.0). For IHC, anti-UCP1 Rabbit Polyclonal (ab10983; Abcam) was used to incubate the sections for 1 h at 37 °C with 1:1000 dilution and then incubated with the biotinylated Goat anti-Rabbit IgG (31820; Invitrogen) with 1:200 dilution for 30 min at 37 °C. Afterward, the sections were incubated with the Horseradish Peroxidase (HRP) Conjugated Streptavidin (N100; Thermo Scientific) at a dilution of 1:200 for 30 min at room temperature and followed by staining with 3,3′-diaminobenzidine tetra-hydrochloride (DAB) staining

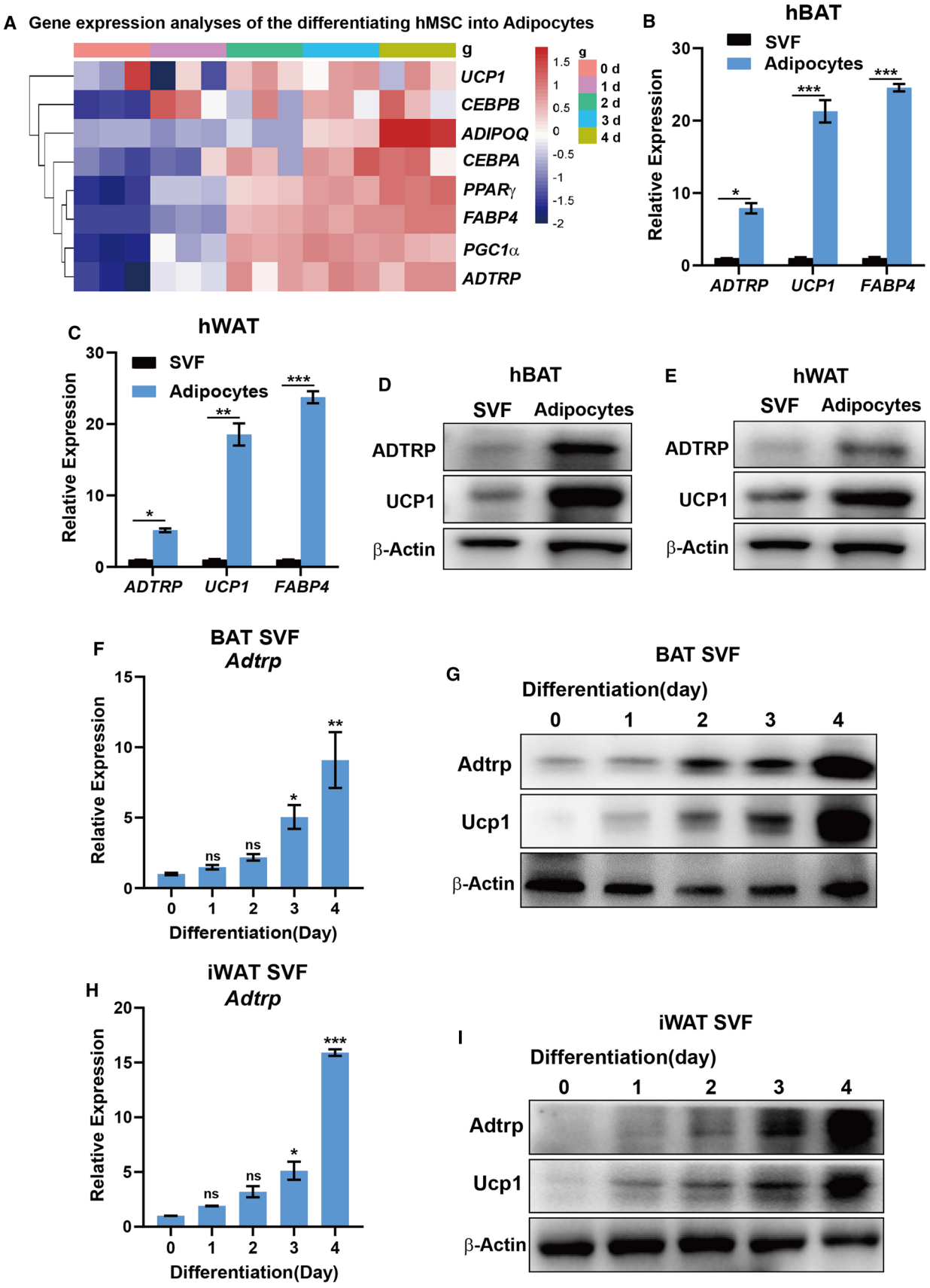
A Gene expression analyses of the differentiating hMSC into Adipocytes
g
UCP1
CEBPB
ADIPOQ
CEBPA
PPARγ
FABP4
PGC1α
ADTRP
1.5
1
0.5
0
-0.5
-1
-1.5
-2
0 d
1 d
2 d
3 d
4 d
B hBAT
SVF
Adipocytes
Relative Expression
ADTRP
UCP1
FABP4
C hWAT
D hBAT
E hWAT
ADTRP
UCP1
β-Actin
F BAT SVF
Adtrp
Differentiation(Day)
G BAT SVF
Differentiation(day)
Adtrp
Ucp1
β-Actin
H iWAT SVF
Adtrp
I iWAT SVF
Differentiation(day)

◂**Fig. 2** Expression of ADTRP in the differentiation process of brown/beige adipocytes. **A** Heat map showing the expressions of *Adtrp* and the marker genes of the adipogenic differentiation process (GEO: GSE80614). **B** and **C** RT-qPCR analyses of *ADTRP*, *UCP1* and *FABP4* in hBAT SVF and hWAT SVF cells after adipogenic differentiation. **D** and **E** Western blot analyses of ADTRP and UCP1 in hBAT SVF and hWAT SVF cells after adipogenic differentiation, β-Actin as the internal control. **F** RT-qPCR analysis of *Adtrp* in mice BAT SVF cells with the adipogenic differentiation process. **G** Western blot analyses of Adtrp and Ucp1 in mice BAT SVF cells with the adipogenic differentiation process, β-Actin as the internal control. **H** RT-qPCR analysis of *Adtrp* in mice iWAT SVF cells with the adipogenic differentiation process. **I** Western blot analyses of Adtrp and Ucp1 in mice iWAT SVF cells with the adipogenic differentiation process, β-Actin as the internal control. Error bars represent the means ± SEM of three independent experiments. *$p < 0.05$, **$p < 0.01$, ***$p < 0.001$, ns: non-statistical significance

kits (Boster, China) according to the manufacturer's instructions. The nucleus was stained with Hematoxylin (Solarbio) for 2 min at 37 °C. The slides were imaged with VENTANA SYSTEM (Roche). The anti-Adtrp antibody was made by ABclonal (China). To generate the anti-Adtrp polyclonal antibody, the peptide fragment of Adtrp (176-193 amino acids, NP_780626.1) was used as antigen to immunize rabbits for producing the anti-Adtrp polyclonal antibody. For IF, anti-Adtrp Rabbit Polyclonal antibody (ABclonal) and anti-S100b Mouse Monoclonal antibody (66616-1-Ig-1-AP; Proteintech, China) were used to incubate the sections with a dilution of 1:200 for 12 h at 4 °C, and then incubated with Alexa Fluor Plus 594-conjugated Goat anti-Rabbit IgG (A32740; Invitrogen) and Fluorescein isothiocyanate (FITC)-conjugated Goat anti-Mouse IgG (F-2761; Invitrogen) with a dilution of 1:500 for 1 h at 37 °C. The nucleus was stained with DAPI 10 μg/mL (Solarbio) for 10 min at 37 °C. The slides were imaged with the A1 confocal laser microscope (Nikon, Japan).

Plasmid construction and transfection

The pCNDA3.1 plasmid was used to express the mouse Adtrp-flag and Adtrp. For S100b, the pEGFP-C3 and pCNDA3.1 plasmids were used to express S100b-GFP and S100b, respectively. For cAMP-responsive element-binding protein 3 (Creb3), the pEGFP-C3 plasmid was used to express the Creb3-GFP. Plasmids were transfected into cells using a Lipofectamine 3000 transfection reagent kit (Invitrogen) based on the manufacturer's instructions.

Western blot and immunoprecipitation (IP) assays

For western blot assay, total protein was extracted by the protein lysis buffer and quantified with a BCA protein quantification kit (Thermo Scientific). Twenty μg total proteins of cell samples or 40 μg total proteins of tissue samples were separated by Sodium Dodecyl Sulfate–Polyacrylamide Gel Electrophoresis (SDS-PAGE), and transferred onto the Polyvinylidene fluoride (PVDF) membrane (Millipore, USA). After incubating with primary antibodies and the corresponding HRP-conjugated secondary antibodies, the substrate of HRP, an enhanced chemiluminescence (ECL) reagent (Thermo Scientific) was used to detect the signal of the membranes. For IP assay, lysis was incubated with the GFP–antibody bond A/G magnetic beads (Sigma-Aldrich) at 4 °C with gentle rotation for 3 h, and the precipitated complex was subjected to western blot analysis as described previously [30]. In this study, the following antibodies were used in western blot and IP assays: anti-β-Actin antibody (AC026, ABclonal), anti-S100b antibody (66616-1-Ig-1-AP; Proteintech), anti-Adtrp antibody (ABclonal), anti-Heat Shock Protein 90 (HSP90) antibody (60318-1-Ig; Proteintech), anti-Ucp1 antibody (ab10983; Abcam), anti-Pparγ antibody (ab178860; Abcam), anti-Flag antibody (AE005, ABclonal), anti-GFP–antibody (66002-1-Ig Proteintech), HRP-conjugated goat anti-rabbit IgG (SA00001-1; Proteintech), and HRP-conjugated goat anti-mouse IgG (SA00001-2; Proteintech).

Oil Red O staining

Cells were fixed with 4% paraformaldehyde for 15 min at 25 °C. Then the cells were stained using the Oil Red O Staining Kit (containing with 0.3% Oil Red O) (Beyotime, China) according to the manufacturer's instructions. After staining, the cells were pictured with a camera (650D, Nikon).

Statistical analysis

All data were expressed as the mean ± SEM (standard error of the mean). Two-tail unpaired or paired Student's t test was applied to analyze the differences between the two groups. The values of *$p < 0.05$, **$p < 0.01$, and ***$p < 0.001$ were indicative of statistical significance and ns was indicative of non-statistical significance. The statistical analysis was performed by GraphPad Prism 8.0. (USA).

Result

Cold exposure or treatment with CL316,243 induced Adtrp expression in mice BAT and iWAT

Cold, as a dominant activator of BAT, via sympathetic nerve controls β3-AR activation and, in turn, induces *Ucp1* mediated non-shivering thermogenesis [13, 31, 32]. CL316,243

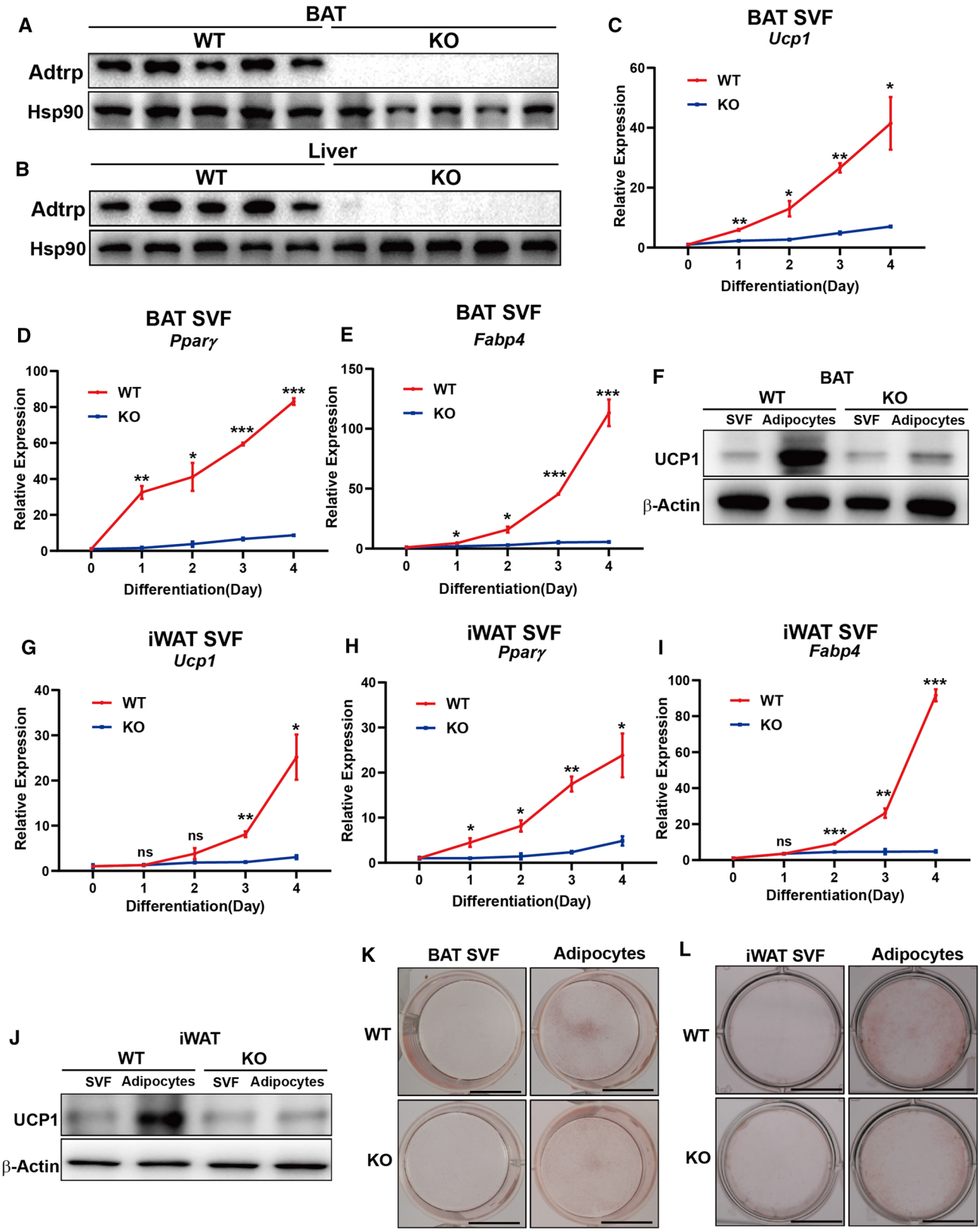
A
BAT
WT
KO
Adtrp
Hsp90
B
Liver
WT
KO
Adtrp
Hsp90
C
BAT SVF
Ucp1
WT
KO
Relative Expression
Differentiation(Day)
D
BAT SVF
Pparγ
WT
KO
Relative Expression
Differentiation(Day)
E
BAT SVF
Fabp4
WT
KO
Relative Expression
Differentiation(Day)
F
BAT
WT
KO
SVF Adipocytes SVF Adipocytes
UCP1
β-Actin
G
iWAT SVF
Ucp1
WT
KO
Relative Expression
Differentiation(Day)
H
iWAT SVF
Pparγ
WT
KO
Relative Expression
Differentiation(Day)
I
iWAT SVF
Fabp4
WT
KO
Relative Expression
Differentiation(Day)
J
iWAT
WT
KO
SVF Adipocytes SVF Adipocytes
UCP1
β-Actin
K
BAT SVF
Adipocytes
WT
KO
L
iWAT SVF
Adipocytes
WT
KO

◂**Fig. 3** *Adtrp* KO effects on the maturation of BAT and beige of iWAT in vitro. **A** and **B** Western blot analysis of Adtrp in BAT and Liver of *Adtrp* KO and WT mice, Hsp90 as the internal control. **C**–**E** RT-qPCR analyses of *Ucp1*, *Pparγ* and *Fabp4* in *Adtrp* KO and WT mice BAT SVF cells with the adipogenic differentiation process. **F** Western blot analysis of *Ucp1* in *Adtrp* KO or WT mice BAT SVF cells after adipogenic differentiation, β-Actin as the internal control. **G**–**I** RT-qPCR analyses of *Ucp1*, *Pparγ* and *Fabp4* in *Adtrp* KO and WT mice iWAT SVF cells with the adipogenic differentiation process. **J** Western blot analysis of Ucp1 in *Adtrp* KO or WT mice iWAT SVF cells after adipogenic differentiation, β-Actin as the internal control. **K** and **L** Oil Red O staining of BAT or iWAT SVF cells in *Adtrp* KO or WT mice before and after adipogenic differentiation (Scale bars, 1 cm). Error bars represent the means ± SEM of three independent experiments. $*p<0.05$, $**p<0.01$, $***p<0.001$; ns, non-statistical significance

as an activator of β3-AR can partially mimic the effects of cold stimulation in mice [33, 34]. By mining the data from the GEO dataset (GEO: GSE86338, GSE104285, GSE13432 and GSE129083), we found five highly expressed genes both in BAT and iWAT after 4℃ or CL316,243 treatment including *Adtrp*, *Glycogen synthase 2* (*Gys2*), *Dio2*, *Ucp1*and *Elongase of very long chain fatty acids-3* (*Elovl3*) (Fig. 1A and S1A-D; Table S2-S5). Due to *Gys2, Dio2, Ucp1* and *Elovl3* have been reported to participate in lipid metabolism [31, 35–37]. We then paid more attention to *Adtrp*. We treated mice at 4℃ or given them intraperitoneal injection of CL316,243, respectively. *Adtrp* was found to be significantly overexpressed in BAT after 7 days of treatment at 4 ℃ (vs. 25 ℃ treated mice as control) or with CL316,243 injections (*vs.* mice with the injection of 0.9% NaCl solution as control) (Fig. 1B–D). Similarly, *Adtrp* was also overexpressed in iWAT after 4℃ or CL316,243 treatment (Fig. 1E–G). Taken together, these results suggested that the *Adtrp* expression could be induced in mice BAT and iWAT by either cold or CL316,243 treatment. The similar expression patterns between *Adtrp* and Ucp1 indicated that *Adtrp* might be involved in the thermogenesis of BAT and beige adipocytes in mice.

Upregulated ADTRP expression in the differentiation process of brown/beige adipocytes

We re-analyzed the data (GEO, GSE80614) about the differentiated process of human mesenchymal stromal cells (hMSCs) to adipocytes [38, 39]. Along with the expressions of the following biomarkers *UCP1, Adiponectin C1Q and collagen domain containing (ADIPOQ), PPARγ*, the expression of *ADTRP* was also up-regulated in the differentiated process of hMSCs (Fig. 2A and Table S6).

To test whether the expression of ADTRP could be up-regulated in the differentiation process, we took advantage of the human hBAT SVF and hWAT SVF cell lines in this study. We found up-regulated ADTRP, both at mRNA and protein levels in mature hBAT and beige hWAT adipocytes (Fig. 2B–E). *UCP1* and *FABP4* as differentiation markers were significantly overexpressed in both mature hBAT and beige hWAT adipocytes (Fig. 2B–E).

We further differentiated the isolated mice BAT SVF and iWAT SVF cells in vitro and found gradual significant increase of *Adtrp* in both brown or beige adipocytes during the process of differentiation, in parallel with the increasing expressions of *Ucp1* (Fig. 2F–I). Overall, these results provided the evidence that *ADTRP* was induced in the differentiated process of human and mice brown/beige adipocytes, which indicated that *ADTRP* might participate in the maturation process of brown/beige adipocytes.

KO of *Adtrp* suppressed the maturation of BAT and beige of iWAT in vitro

To further investigate the functions of *Adtrp* in mice, we successfully generated an *Adtrp* KO mouse with a deletion in exon 2 to exon 4 of *Adtrp* genomic loci via using the CRISPR/Cas9 system (Fig. S2A and B). *Adtrp* KO mice BAT and liver tissues were completely devoid of *Adtrp* expression (Fig. 3A and B; S2C and D).

To confirm whether *Adtrp* was essential in the differentiation process of BAT and iWAT in vitro, we analyzed the BAT SVF and iWAT SVF cells isolated from *Adtrp* KO mice. *Ucp1*, *Pparγ* and *Fabp4* in *Adtrp* KO BAT SVF cells were significantly decreased compared with the WT cells in the differentiation process (Fig. 3C–E). The protein levels of Ucp1 in the mature *Adtrp* KO BAT SVF adipocytes was also markedly lower than that in the WT cells (Fig. 3F). Consistently, the expressions of *Ucp1*, *Pparγ* and *Fabp4* were also significantly reduced in *Adtrp* KO iWAT SVF cells compared with the WT cells during the differentiation process of the iWAT SVF cells, where the protein levels of Ucp1 in the *Adtrp* KO iWAT adipocytes were also lower than that of the WT cells (Fig. 3G–J). Accordingly, the lipid accumulations of the mature *Adtrp* KO BAT SVF adipocytes were decreased compared with the WT adipocytes (Fig. 3K–L). Overall, we demonstrated that the maturation of BAT and beige iWAT in *Adtrp* KO mice were suppressed, which indicated the fundamental role of *Adtrp* in the maturation process of BAT and beige iWAT in mice.

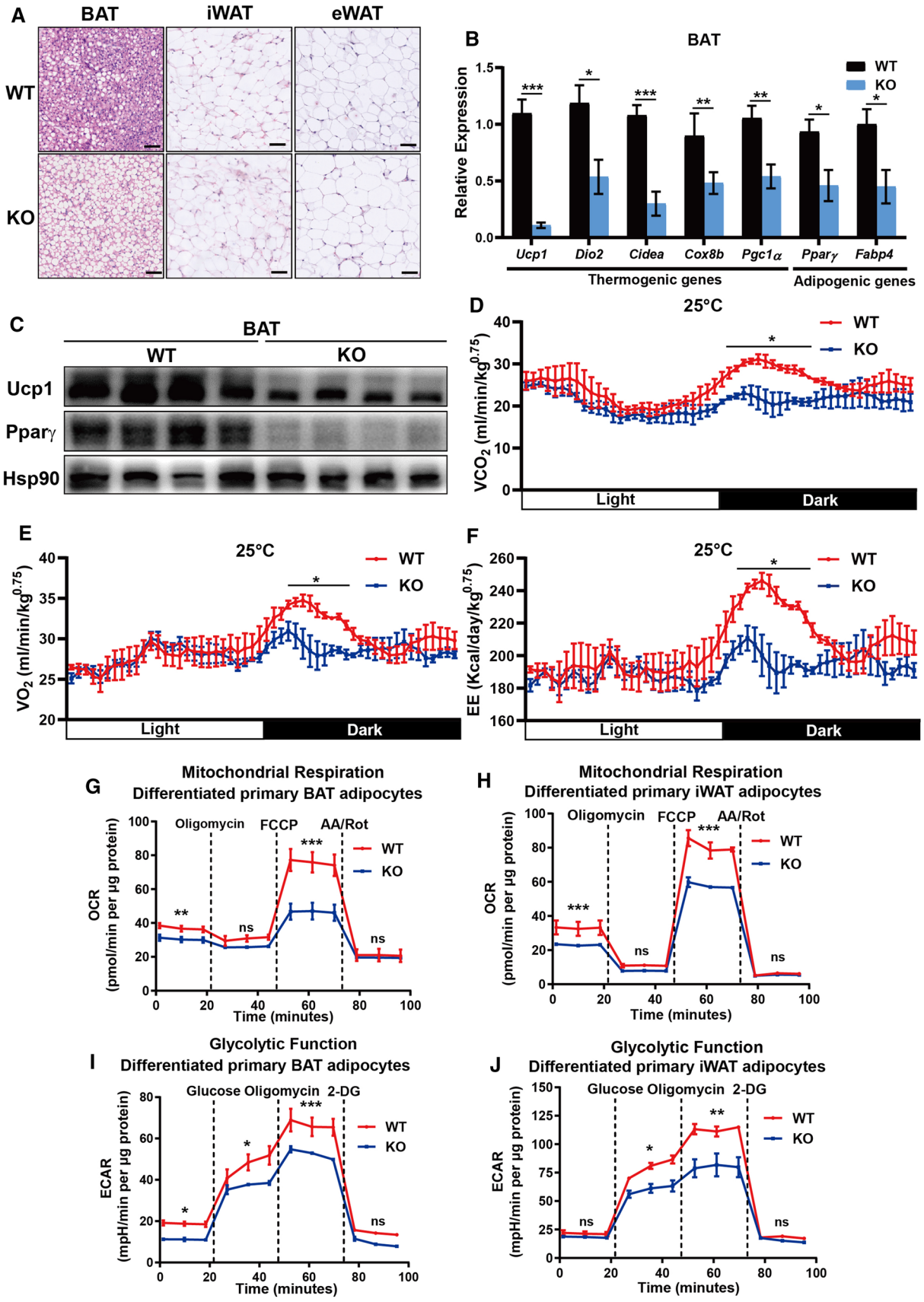
A
BAT
iWAT
eWAT
WT
KO
B
BAT
Relative Expression
WT
KO
Ucp1
Dio2
Cidea
Cox8b
Pgc1α
Pparγ
Fabp4
Thermogenic genes
Adipogenic genes
C
BAT
WT
KO
Ucp1
Pparγ
Hsp90
D
25°C
VCO2 (ml/min/kg0.75)
Light
Dark
E
25°C
VO2 (ml/min/kg0.75)
Light
Dark
F
25°C
EE (Kcal/day/kg0.75)
Light
Dark
G
Mitochondrial Respiration
Differentiated primary BAT adipocytes
OCR (pmol/min per µg protein)
Oligomycin
FCCP
AA/Rot
Time (minutes)
H
Mitochondrial Respiration
Differentiated primary iWAT adipocytes
OCR (pmol/min per µg protein)
Oligomycin
FCCP
AA/Rot
Time (minutes)
I
Glycolytic Function
Differentiated primary BAT adipocytes
ECAR (mpH/min per µg protein)
Glucose
Oligomycin
2-DG
Time (minutes)
J
Glycolytic Function
Differentiated primary iWAT adipocytes
ECAR (mpH/min per µg protein)
Glucose
Oligomycin
2-DG
Time (minutes)

◂**Fig. 4** *Adtrp* KO effects on the accumulation of lipid excess in BAT and metabolic disorders in mice. **A** Histopathological images of BAT, iWAT and eWAT from *Adtrp* KO mice and WT mice at the age of 8 weeks, ($n=4$, Scale bars, 50 μm). **B** RT-qPCR analyses of *Ucp1, Dio2, Cidea, Cox8b, Pgc1a, Pparγ* and *Fabp4* in BAT of *Adtrp* KO and WT mice ($n=5$). **C** Western blot analyses of Ucp1 and Pparγ in BAT of *Adtrp* KO or WT mice, Hsp90 as the internal control ($n=4$). **D**–**F** VCO_2 generation, VO_2 consumption and EE of *Adtrp* KO and WT mice in metabolic cages at the age of 8 weeks ($n=6$). **G** and **H** OCR analyses of the mitochondrial respiration in *Adtrp* KO and WT differentiated BAT or iWAT SVF adipocytes. **I** and **J** ECAR analyses of glycolytic functions in *Adtrp* KO and WT differentiated BAT or iWAT SVF adipocytes. Error bars represent the means ± SEM of three independent experiments. *$p<0.05$, **$p<0.01$, ***$p<0.001$; ns, non-statistical significance

KO of *Adtrp* caused accumulation of lipid excess of BAT and metabolic disorder in mice

We used further *Adtrp* KO mice to demonstrate the role of *Adtrp* in the adipose tissues in vivo. There was no significant difference in the body weights between *Adtrp* KO and WT mice with normal chow diet (Fig. S3A). Next, we examined the histopathology of the adipose and liver tissues from *Adtrp* KO and WT mice. There were abundant lipid accumulated areas in BAT in *Adtrp* KO mice, compared with the WT mice; as well as no morphological differences of iWAT, eWAT and liver in between WT and *Adtrp* KO mice (Fig. 4A and S3B). The thermogenic genes (*Ucp1, Dio2, Cidea, Cox8b, Pgc1α* and adipogenic genes (*Pparγ and Fabp4*) were significantly downregulated in BAT of *Adtrp* KO mice (Fig. 4B). Consistently, we also found notably decreased Ucp1 and Pparγ expressions in *Adtrp* KO mice, which suggested that the deletion of *Adtrp* may impair the thermogenesis and metabolism in mice (Fig. 4C). Accordingly, using the metabolic cages, we observed the significant decreases of VCO_2 generation, VO_2 consumption, and EE in *Adtrp* KO mice from nightfall to midnight at 25 °C compared with the WT mice (Fig. 4D–F). There was no difference in food or water intake between the *Adtrp* KO and WT mice at 25 °C (Fig. S3C and D). There was also no difference in the glucose tolerance and insulin sensitivity between the *Adtrp* KO and WT mice (Fig. S3E and F).

Furthermore, the results of the mitochondrial stress OCR tests showed that the differentiated *Adtrp* KO BAT-SVF and iWAT-SVF adipocytes exhibited significant decline in basal respiration, maximal respiration and spare respiration capacity tests compared with the WT cells in vitro (Fig. 4G and H; S3G and H). Meanwhile, the ATP-linked respiration of the differentiated *Adtrp* KO iWAT-SVF cells was significantly decreased compared with the WT cells (Fig. S3H). The results of the glycolysis stress ECAR tests demonstrated that glycolysis, glycolytic capacity as well as glycolytic reserve were decreased in the differentiated *Adtrp* KO BAT-SVF and iWAT-SVF cells compared with the WT cells (Fig. 4I and J; S3I and J). In this context, our results demonstrated that KO of *Adtrp* resulted in lipid excess accumulation in BAT and impaired the metabolic homeostasis both in vitro and in vivo.

KO of *Adtrp* suppressed the thermogenesis of BAT and beige iWAT in mice

To further illustrate the influence of *Adtrp* on thermogenic functions in vivo, we treated mice with acute cold (4 °C for 8 h). The core temperatures of *Adtrp* KO mice decreased dramatically and thermal images also showed that the surface temperatures of *Adtrp* KO mice dropped much faster than WT mice (Fig. 5A and B).

Next, we then exposed the mice with 16 °C for 7 days. The histological images showed that the lipid droplet areas of BAT, iWAT and eWAT in *Adtrp* KO mice were more abundant than those of WT mice exposed to 16 °C for 7 days (Fig. 5C). The expressions of thermogenic-related genes (such as *Ucp1*, *Dio2*, *Cidea*, *Cox8b*, *Pgc1α*, *Pparγ* and *Prdm16*) were also at significantly lower levels in BAT and beige iWAT in *Adtrp* KO mice than those of WT mice after the treatment of 16 °C for 7 days (Fig. 5D–G). Consistently, using the metabolic cages at 16 °C, we observed that the metabolism of *Adtrp* KO mice was impaired with the dramatically decrease in VCO_2 generation, VO_2 consumption, and EE (Fig. 5H and I; Fig. S4A). There was no significant difference in food or water intake between the *Adtrp* KO and WT mice at 16 °C (Fig. S4B and C). The Area Under Curve (AUC) analyses showed that the metabolic capabilities (VCO_2 generation, VO_2 consumption, and EE) of *Adtrp* KO mice were not increased as much as in WT mice in 16 °C compared with 25 °C (Fig. 5J and K; Fig. S4D). Taken together, these results showed that the metabolism and thermogenesis of BAT and beige iWAT were impaired in *Adtrp* KO mice.

CL316,243 treatment recovered the thermogenesis of BAT and beige iWAT in *Adtrp* KO mice

To further detect whether *Adtrp* directly participated in thermogenesis through stimulation of β3-AR in BAT and beige iWAT, we intraperitoneally injected the β3-AR agonist CL316,243 to *Adtrp* KO and WT mice for 7 days. Unexpectedly, when we exposed these mice to acute cold (4 °C for 8 h), the core temperatures of *Adtrp* KO mice did not have any difference compared with the WT mice (Fig. S4E). Histopathological images showed no morphological differences

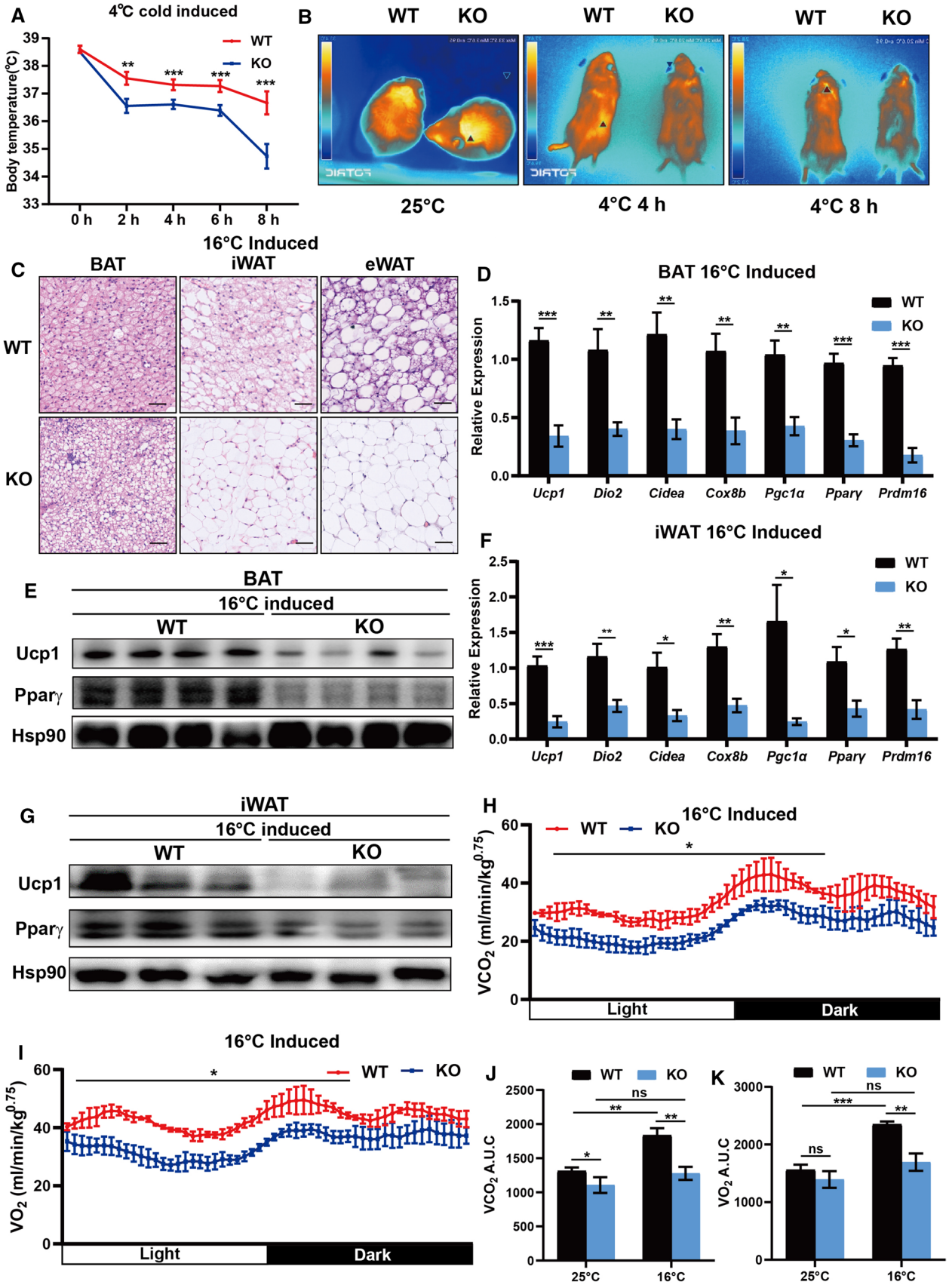
A
4℃ cold induced
Body temperature(℃)
WT
KO
0 h
2 h
4 h
6 h
8 h
B
WT
KO
25°C
4°C 4 h
4°C 8 h
C
16°C Induced
BAT
iWAT
eWAT
WT
KO
D
BAT 16°C Induced
Relative Expression
Ucp1
Dio2
Cidea
Cox8b
Pgc1α
Pparγ
Prdm16
E
BAT
16°C induced
Ucp1
Pparγ
Hsp90
F
iWAT 16°C Induced
G
iWAT
H
16°C Induced
VCO2 (ml/min/kg0.75)
Light
Dark
I
VO2 (ml/min/kg0.75)
J
VCO2 A.U.C
K
VO2 A.U.C
ns

◂**Fig. 5** *Adtrp* KO effects on the thermogenesis of BAT and beige iWAT in mice. **A** The core body temperatures of *Adtrp* KO and WT mice at different time points after exposure to 4 °C ($n=10$). **B** Thermal images of *Adtrp* KO and WT mice at different time points after exposure to 4 °C ($n=6$). **C** Histological images of BAT, iWAT and eWAT from *Adtrp* KO mice and WT mice at the age of 8 weeks with 16 °C exposure for 7 days ($n=4$, Scale bars, 50 μm). **D** RT-qPCR analyses of *Ucp1, Dio2, Cidea, Cox8b, Pgc1α, Pparγ* and *Prdm16* in BAT of *Adtrp* KO and WT mice with 16 °C exposure for 7 days ($n=5$). **E** Western blot analyses of Ucp1 and Pparγ in BAT of *Adtrp* KO or WT mice with 16 °C exposure for 7 days, Hsp90 as the internal control ($n=4$). **F** RT-qPCR analyses of *Ucp1, Dio2, Cidea, Cox8b, Pgc1α, Pparγ* and *Prdm16* in iWAT of *Adtrp* KO and WT mice with 16 °C exposure for 7 days ($n=5$). **G** Western blot analyses of Ucp1 and Pparγ in iWAT of *Adtrp* KO and WT mice with 16 °C exposure for 7 days, Hsp90 as the internal control ($n=3$). **H–I** VCO_2 generation, VO_2 consumption of *Adtrp* KO and WT mice in metabolic cages at the age of 8 weeks with 16 °C exposure ($n=6$). **J–K** Statistics of AUC data of VCO_2 and VO_2 about *Adtrp* KO and WT mice at 25 °C and 16 °C. Error bars represent the means ± SEM of three independent experiments. $^{*}p<0.05$, $^{**}p<0.01$, $^{***}p<0.001$; ns, non-statistical significance

in BAT, iWAT and eWAT between the WT and *Adtrp* KO mice after 7 days of CL 316,243 treatment (Fig. 6A).

There was no significant difference in the expression profile of thermogenic genes in BAT and beige iWAT between the *Adtrp* KO and WT mice treated with CL316,243 (Fig. 6B–E). This indicated that the thermogenic functions of *Adtrp* KO mice recovered after 7 days' of CL316,243 treatment. Moreover, we found no significant differences in serum TG and FFA levels of *Adtrp* KO mice compared with the WT mice at 25 °C, whereas the TG and FFA levels of *Adtrp* KO mice were significantly higher than those of WT mice at 16 °C for 7 days. TG and FFA levels of *Adtrp* KO mice were significantly lower than those of the WT mice after 7 days' of CL316,243 treatment (Fig. 6F and G), which indicated CL316,243 treatment activated the lipid metabolism and thermogenesis of *Adtrp* KO mice. In addition, the immunohistological analysis images also showed that the expression of Ucp1 in BAT and iWAT of *Adtrp* KO mice was significantly less abundant than those of the WT mice, both at 25 °C and 16 °C. However, there was no significant difference in the expression of Ucp1 between the *Adtrp* KO and WT mice after 7 days' CL316,243 treatment (Fig. 6H and I). These results demonstrated that the CL316,243 treatment could recover the thermogenesis of BAT and beige iWAT in *Adtrp* KO mice.

Adtrp mediated the secretion of S100b in BAT and iWAT of mice

To understand how *Adtrp* may impact the β3-AR mediating thermogenesis, we searched the NCBI database, and found 5 possible protein candidates (CKLF like MARVEL transmembrane domain containing 7 [CMTM7], [CREB3], S100B, Transmembrane p24 trafficking protein family member 8 [TMED8] and Vitronectin [VTN]), which may interact with the Adtrp [40–42] (Fig. S5A). There has been reports suggesting *Creb3* and *S100b* to participate in the metabolism of adipose tissues [43, 44]. Using IP analysis, we confirmed that Adtrp could interact with S100b instead of Creb3 (Fig. 7A and Fig. S5B). We also observed that KO of *Adtrp* did not impact the expression of *S100b* in mice BAT and iWAT (Fig. 7B and C; Fig. S5C and D).

It has been demonstrated that S100b could be secreted from thermogenic adipocytes to process the neurotrophic effects on the sympathetic innervations of BAT and beige iWAT to stimulate the β3-AR mediated activation of thermogenesis [45]. Thereafter, we hypothesized that Adtrp might bind to the S100b and mediate the secretion of S100b. To verify this hypothesis, we collected the conditional medium from the differentiated BAT and iWAT SVF adipocytes. We found that the secretion of S100b in *Adtrp* KO adipocytes was significantly lower than that in the WT adipocytes with the similar expression patterns of S100b in BAT and iWAT adipocytes (Fig. 7D–G). Consistently, we also showed that Adtrp could mediate the secretion of S100b in 293T cells (Fig. 7H and I). Moreover, the immunofluorescence staining analyses of Adtrp (Red) and S100b (Green) showed the co-localization of Adtrp and S100b in BAT and iWAT (Fig. 7J). Together, these findings demonstrated that Adtrp could regulate the thermogenic functions of BAT and iWAT by mediating the secretion of S100b in mice.

Discussion

BAT and beige WAT plays key regulatory role in metabolism and non-shivering thermogenesis in small mammals and humans [46, 47]. In this study, we determined that *Adtrp* was significantly up-regulated in the differentiated brown/beige adipocytes and in the thermogenic process of BAT and beige iWAT in mice. Moreover, the *Adtrp* KO mice showed the metabolic disorders and cold intolerance with significantly lower expressions of thermogenic genes, and β3-AR agonist CL316,243 treatment could recover the thermogenesis of BAT and beige iWAT in *Adtrp* KO mice. Overall, we demonstrated that *Adtrp* might serve as a novel fundamental key regulator of metabolism, especially in the thermogenesis of adipose tissues.

The multiple functions of *ADTRP* have been reported by several studies as stated below. *ADTRP* acted as a CAD susceptibility gene [17], and ADTRP also regulated the

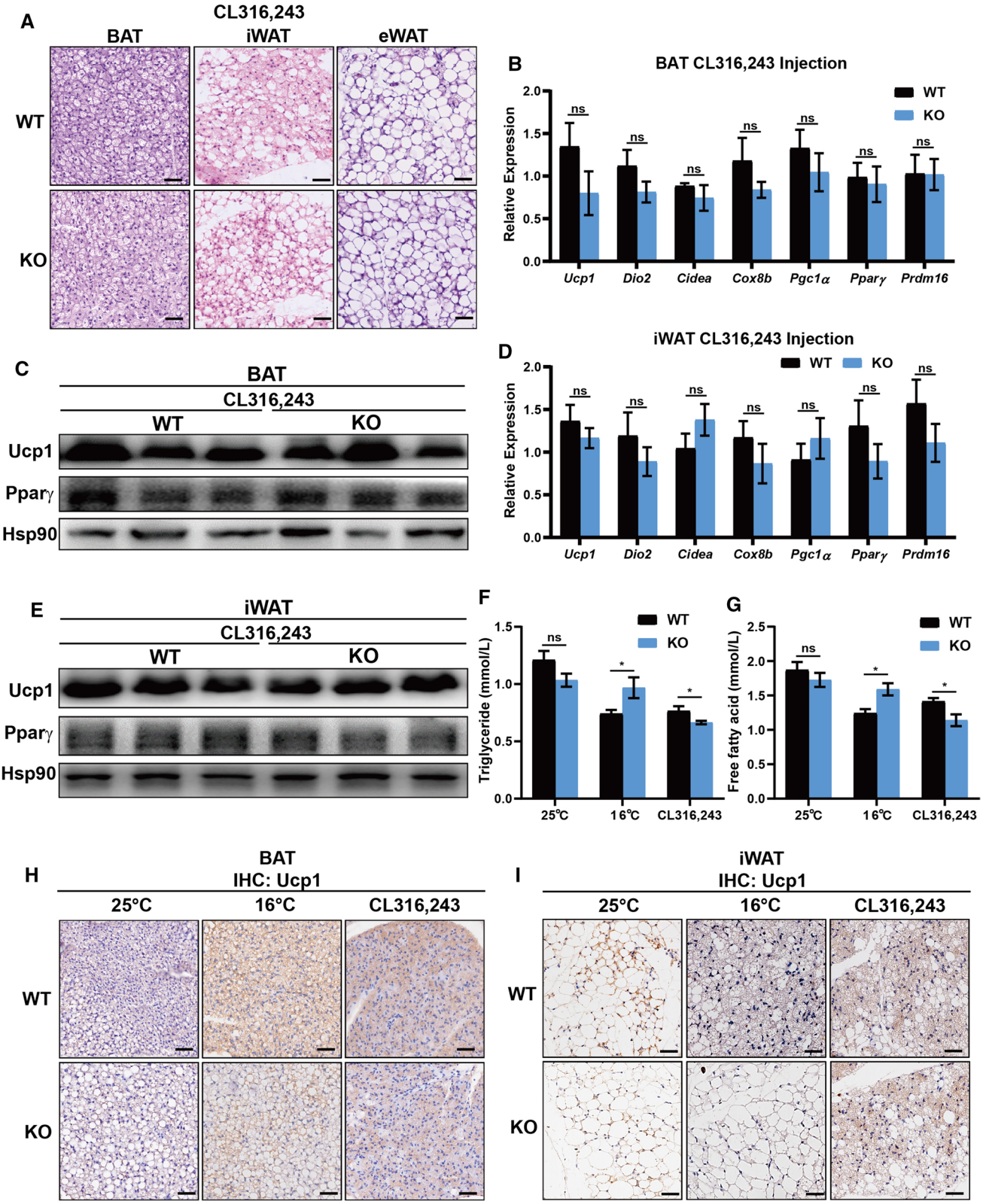
A
CL316,243
BAT
iWAT
eWAT
WT
KO
B
BAT CL316,243 Injection
WT
KO
Relative Expression
ns
Ucp1
Dio2
Cidea
Cox8b
Pgc1α
Pparγ
Prdm16
C
BAT
CL316,243
WT
KO
Ucp1
Pparγ
Hsp90
D
iWAT CL316,243 Injection
E
iWAT
F
Triglyceride (mmol/L)
25℃
16℃
CL316,243
G
Free fatty acid (mmol/L)
H
BAT
IHC: Ucp1
I
iWAT

◂**Fig. 6** CL316,243 treatment effects on the potential recovery of the thermogenesis in BAT and beige iWAT of *Adtrp* KO mice. **A** Histopathological images of BAT, iWAT and eWAT from *Adtrp* KO mice and WT mice at age of 8 weeks with CL316,243 injections for 7 days ($n=4$, Scale bars, 50 μm). **B** RT-qPCR analyses of *Ucp1, Dio2, Cidea, Cox8b, Pgc1α, Pparγ* and *Prdm16* in BAT of *Adtrp* KO and WT mice with CL316,243 treatment for 7 days ($n=5$). **C** Western blot analyses of Ucp1 and Pparγ in BAT of *Adtrp* KO or WT mice with CL316,243 treatment for 7 days, Hsp90 as the internal control ($n=3$). **D** RT-qPCR analysis of *Ucp1, Dio2, Cidea, Cox8b, Pgc1α, Pparγ* and *Prdm16* in iWAT of *Adtrp* KO and WT mice with CL316,243 treatment for 7 days ($n=5$). **E** Western blot analyses of the expression of Ucp1 and Pparγ in iWAT of *Adtrp* KO and WT mice with CL316,243 treatment for 7 days, Hsp90 as the internal control ($n=3$). **F** and **G** The levels of TG and FFA in the serum of *Adtrp* KO and WT mice with 16 °C exposure for 7 days or CL316,243 treatment for 7 days ($n=5$). **H** and **I** IHC images of Ucp1 in BAT and iWAT of *Adtrp* KO and WT mice with 16 °C exposure for 7 days or CL316,243 treatment for 7 days ($n=4$, scale bars, 50 μm). Error bars represent the means ± SEM of three independent experiments. $^*p<0.05$, ns: non-statistical significance

anticoagulant protection of ECs and participated in the vascular development, integrity and stability [20, 21]. Furthermore, ADTRP served as an atypical hydrolytic enzyme to hydrolyze FAHFAs [22, 23]. Hereby, we found a novel unprecedented function of *Adtrp*, its participation in the metabolism of adipose tissues, especially in the regulation of the non-shivering thermogenesis in mice.

The noradrenaline, released by SNS, activates the β3-AR pathway, in turn to drive the non-shivering thermogenesis of BAT and beige iWAT in mice [48–50]. Researchers have reported that some genes could mediate the activations of BAT and beige iWAT via regulating the sympathetic innervations in mice. A study has shown that the adipose-specific ablation of *Prdm16* resulted in a decrease in the sympathetic innervations of beige iWAT [51]. Recently, another study has shown that *Calsyntenin 3β* (*Clstn3β*) mediated the secretion of S100b, which posed a neurotrophic factor, enhancing the sympathetic innervations of BAT and beige iWAT [45]. Consistent with this study, we demonstrated that Adtrp could bind to S100b and mediate the secretion of S100b, which in turn promoted β3-AR mediated thermogenesis via enhancing the sympathetic innervations of BAT and beige iWAT in mice. The secretion pathway of S100b might be driven by the Clstn3β in the endoplasmic reticulum and Adtrp in the cytomembrane.

When mice were exposed to cold, the serum TG and FFA were transported to BAT and beige iWAT for non-shivering thermogenesis [52]. However, in our study, we showed that serum TG and FFA of *Adtrp* KO mice were not consumed as much as WT in a long-term 16 °C exposure, which indicated that the thermogenic function of *Adtrp* KO mice was restrained.

A previous study has suggested that ADTRP involves in the osteogenic differentiation of bone marrow MSC (BM-MSC) with the osteogenic medium. However, no any differences in bone/cartilage/oral cleft between *Adtrp* KO and WT mice were found [21]. In contrast to this study, we showed that *Adtrp* was essential in the differentiation process of mice brown/beige adipocytes. In addition, *Adtrp* KO caused the dysplasia of BAT with an accumulation of lipid excess in mice. The discrepancy between the osteogenic and adipogenic differentiation might be due to the complex roles of *Adtrp* in different tissues at different developmental periods.

Studies have demonstrated that androgen induced high expression of ADTRP in ECs could inhibit the atherosclerotic process [20, 53]. Another study showed that PPARγ transcriptionally activated the expression of *ADTRP* in monocytes/macrophages and human atherosclerotic plaques [54]. Different from these studies, we demonstrated that cold exposure or β3-AR agonist CL316,243 treatment could induce the expression of Adtrp. We did not find any phenotypic differences between female and male *Adtrp* KO mice, which indicated that the functions of *Adtrp* in thermogenic adipose tissues were androgen independent. Future studies by generating conditional adipose tissues *Adtrp* KO mice might extend our knowledge on the precise role of *Adtrp* in the metabolism of adipose tissues.

Earlier few studies have illustrated that suppressing the BAT thermogenic capacity might damage the glucose homeostasis. However, in our current study, we found that there were no significant changes in body weights, serum biochemical indices, glucose tolerances or insulin sensitivities between WT and KO mice at 25 °C with regular chow diet. Consistent with our results, a recent study also failed to find any significant differences in glucose tolerances or insulin sensitivities between *Adtrp* KO and WT mice with high-fat diet (HFD) [23]. We got similar results on the glucose homeostasis of *Adtrp* KO mice, which may indicate that *Adtrp* is not associated with the process of obesity and diabetes. Similar to *Adtrp* KO data, *Estrogen-related receptor gamma (ERRγ)* KO mice exhibited a pronounced whitening of BAT and a decrease of thermogenic capacity, without any changes in body weight, glucose tolerances, insulin sensitivities with chow diet or HFD [55]. We speculated that there might be a compensating effect of the glucose homeostasis in *Adtrp* KO mice. *Adtrp* KO inhibited the hydrolysis of FAHFAs in mice adipocytes and the high level of FAHFAs could enhance insulin-stimulated glucose uptake [23, 24]. On the other hand, deletion of *Adtrp* caused accumulation of lipid excess in BAT and metabolic disorders, which might lead to further glucose intolerance in mice. This dual-function of *Adtrp* might

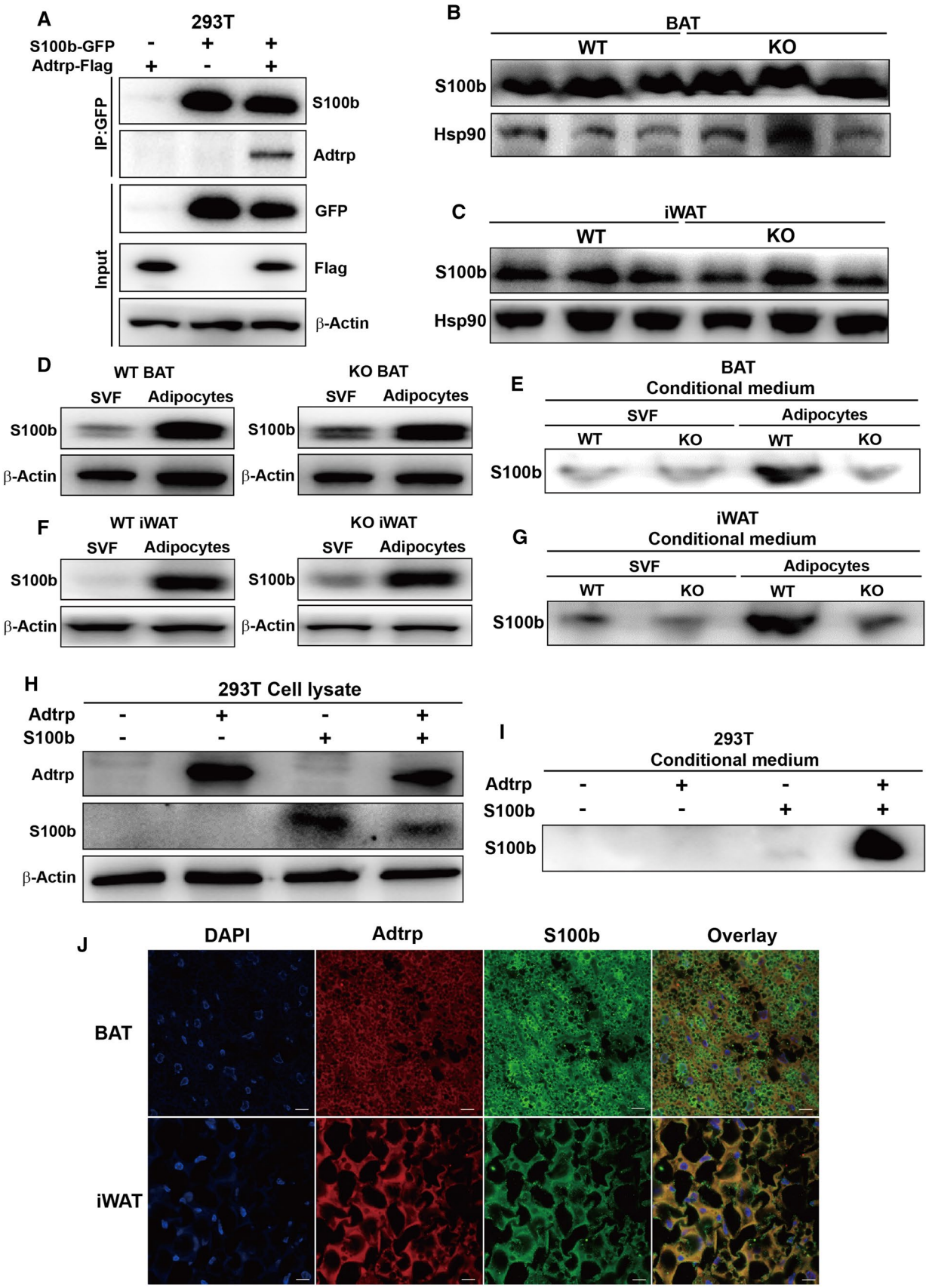
A
293T
S100b-GFP - + +
Adtrp-Flag + - +
IP:GFP
S100b
Adtrp
Input
GFP
Flag
β-Actin
B
BAT
WT KO
S100b
Hsp90
C
iWAT
WT KO
S100b
Hsp90
D
WT BAT
SVF Adipocytes
S100b
β-Actin
KO BAT
SVF Adipocytes
S100b
β-Actin
E
BAT
Conditional medium
SVF Adipocytes
WT KO WT KO
S100b
F
WT iWAT
SVF Adipocytes
S100b
β-Actin
KO iWAT
SVF Adipocytes
S100b
β-Actin
G
iWAT
Conditional medium
SVF Adipocytes
WT KO WT KO
S100b
H
293T Cell lysate
Adtrp - + - +
S100b - - + +
Adtrp
S100b
β-Actin
I
293T
Conditional medium
Adtrp - + - +
S100b - - + +
S100b
J
DAPI
Adtrp
S100b
Overlay
BAT
iWAT

◂**Fig. 7** Adtrp mediated secretion of S100b in BAT and iWAT of mice. **A** IP by anti-GFP–antibody bond A/G magnetic beads, and Western blot analyses of S100b and Adtrp in 293T cells. **B** and **C** Western blot analysis of S100b in BAT and iWAT of *Adtrp* KO or WT mice, Hsp90 as the internal control ($n=3$). **D** Western blot analysis of S100b in *Adtrp* KO or WT mice BAT SVF cells after adipogenic differentiation, β-Actin as the internal control. **E** Western blot analysis of S100b in a conditional medium of *Adtrp* KO or WT mice BAT SVF cells after adipogenic differentiation. **F** Western blot analysis of S100b in *Adtrp* KO or WT mice iWAT SVF cells after adipogenic differentiation, β-Actin as the internal control. **G** Western blot analysis of S100b in a conditional medium of in *Adtrp* KO or WT mice SVF iWAT SVF cells after adipogenic differentiation. **H** Western blot analyses of Adtrp and S100b in different Adtrp or S100b expressed 293T cells, β-Actin as the internal control. **I** Western blot analysis of S100b in a conditional medium in different Adtrp or S100b expressed 293T cells. **J** Immunofluorescence staining analyses of Adtrp (Red), S100b (Green), and nucleus (Blue) in mice BAT and iWAT (scale bars, 10 μm)

balance and maintain the normal glucose metabolism in *Adtrp* KO mice.

ADTRP is a CAD susceptibility gene and a single-nucleotide polymorphism (SNP) of rs6903956 is associated with the low expression of *ADTRP* in human [17]. Some studies have shown that perivascular adipose tissue (PVAT) was similar to classical BAT, and associated with CAD, especially, in the development of atherosclerosis in the aorta [56–58]. A study has shown that BAT-Specific *PPARγ* KO impaired the development of PVAT and aggravated the atherosclerosis in mice [59]. In line with the above studies, one could assume that ADTRP might affect the occurrence of CAD via regulating the functions of PVAT and BAT in human.

One of the limitations of our present study was that we did not study the functions of *Adtrp* in PVAT and CAD in mice. In future, further studies, such analyses of the PVAT and CAD in *Adtrp* KO mice, as well as to establish the mice model of CAD and atherosclerosis to study the relations between *ADTRP* and CAD should be done. Another limitation of this study could be that we did not investigate the clinical metabolic disorders related to CAD. We are going to collect the samples from the metabolic disorders related to CAD patients and record the corresponding follow-up information to investigate the relationship between ADTRP and the metabolic disorders related to CAD in our future project.

In summary, the present study demonstrated that *Adtrp* could be a novel fundamental regulator of the differentiation and thermogenesis of BAT and beige iWAT. *Adtrp* mediated the secretion of S100b to promote the β3-AR mediated thermogenesis via enhancing the sympathetic innervations of BAT and beige iWAT in mice (summarized in Fig. 8).

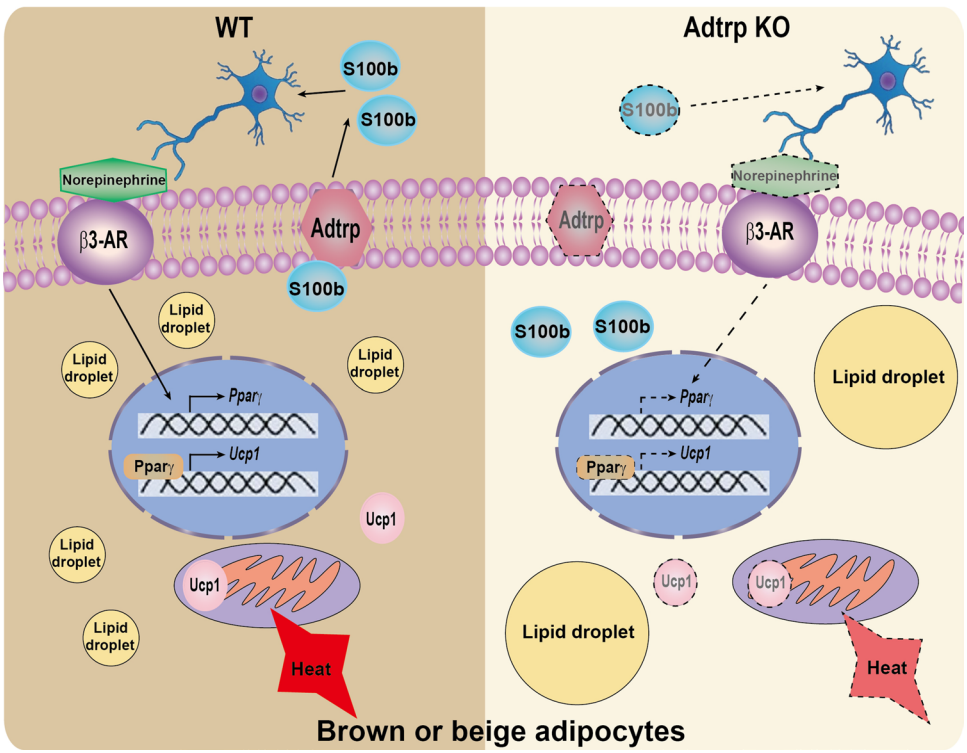

Fig. 8 A proposed working model of Adtrp action in brown and beige adipose tissues. Adtrp mediates the secretion of S100b to promote the β3-AR mediated thermogenesis via enhancing the sympathetic innervation of BAT and beige iWAT in mice

Supplementary Information The online version contains supplementary material available at https://doi.org/10.1007/s00018-022-04441-9.

Acknowledgements We thank professor Fazheng Ren from China Agricultural University for providing guidance for the experiments. We thank professor Nafis A Rahman from University of Turku for the language editing.

Author's contributions XL designed the study concept and supervised the project and analyzed the data. PL, RS and XL interpreted the data. PL, RS and YD conducted the experiments. PL, RS and HL analyzed RNA-seq and microarray data. All authors approved the final content.

Funding This study was supported by grants from the National Natural Science Foundation of China (82171854 and 31970802), Beijing Municipal Natural Science Foundation (7202099) and the Medical University of Bialystok, Poland (SUB/1/DN/20/006/1104, to Xiangdong Li).

Availability of data and material The datasets or materials generated in the current study are available on reasonable request.

Declarations

Conflict of interests The authors declare that they have no conflict of interest.

Ethics approval All animal studies were approved by the ethical committee of the China Agricultural University (No.: AW32201202-3-2).

Consent to participate Not applicable. No human subjects were recruited for this study.

Consent for publication Not applicable.

References

1. Seale P, Lazar MA (2009) Brown fat in humans: turning up the heat on obesity. Diabetes 58(7):1482–1484
2. Lo KA, Sun L (2013) Turning WAT into BAT: a review on regulators controlling the browning of white adipocytes. Biosci Rep 33:5
3. Seale P, Bjork B, Yang W, Kajimura S, Chin S, Kuang S, Scimè A, Devarakonda S, Conroe HM, Erdjument-Bromage H et al (2008) PRDM16 controls a brown fat/skeletal muscle switch. Nature 454(7207):961–967
4. Cannon B, Nedergaard J (2004) Brown adipose tissue: function and physiological significance. Physiol Rev 84(1):277–359
5. Golozoubova V, Hohtola E, Matthias A, Jacobsson A, Cannon B, Nedergaard J (2001) Only UCP1 can mediate adaptive nonshivering thermogenesis in the cold. FASEB J 15(11):2048–2050
6. Nedergaard J, Golozoubova V, Matthias A, Asadi A, Jacobsson A, Cannon B (2001) UCP1: the only protein able to mediate adaptive non-shivering thermogenesis and metabolic inefficiency. Biochem Biophys Acta 1504(1):82–106
7. Wu J, Bostrom P, Sparks LM, Ye L, Choi JH, Giang AH, Khandekar M, Virtanen KA, Nuutila P, Schaart G et al (2012) Beige adipocytes are a distinct type of thermogenic fat cell in mouse and human. Cell 150(2):366–376
8. Cypess AM, Lehman S, Williams G, Tal I, Rodman D, Goldfine AB, Kuo FC, Palmer EL, Tseng YH, Doria A et al (2009) Identification and importance of brown adipose tissue in adult humans. N Engl J Med 360(15):1509–1517
9. Virtanen KA, Lidell ME, Orava J, Heglind M, Westergren R, Niemi T, Taittonen M, Laine J, Savisto NJ, Enerbäck S et al (2009) Functional brown adipose tissue in healthy adults. N Engl J Med 360(15):1518–1525
10. Vitali A, Murano I, Zingaretti MC, Frontini A, Ricquier D, Cinti S (2012) The adipose organ of obesity-prone C57BL/6J mice is composed of mixed white and brown adipocytes. J Lipid Res 53(4):619–629
11. Harms M, Seale P (2013) Brown and beige fat: development, function and therapeutic potential. Nat Med 19(10):1252–1263
12. Himms-Hagen J, Melnyk A, Zingaretti MC, Ceresi E, Barbatelli G, Cinti S (2000) Multilocular fat cells in WAT of CL-316243-treated rats derive directly from white adipocytes. Am J Physiol Cell Physiol 279(3):C670-681
13. Collins S (2011) β-adrenoceptor signaling networks in adipocytes for recruiting stored fat and energy expenditure. Front Endocrinol (Lausanne) 2:102
14. Jimenez M, Léger B, Canola K, Lehr L, Arboit P, Seydoux J, Russell AP, Giacobino JP, Muzzin P, Preitner F (2002) Beta(1)/beta(2)/beta(3)-adrenoceptor knockout mice are obese and cold-sensitive but have normal lipolytic responses to fasting. FEBS Lett 530(1–3):37–40
15. Bachman ES, Dhillon H, Zhang CY, Cinti S, Bianco AC, Kobilka BK, Lowell BB (2002) betaAR signaling required for diet-induced thermogenesis and obesity resistance. Science 297(5582):843–845
16. Robidoux J, Martin TL, Collins S (2004) Beta-adrenergic receptors and regulation of energy expenditure: a family affair. Annu Rev Pharmacol Toxicol 44:297–323
17. Wang F, Xu CQ, He Q, Cai JP, Li XC, Wang D, Xiong X, Liao YH, Zeng QT, Yang YZ et al (2011) Genome-wide association identifies a susceptibility locus for coronary artery disease in the Chinese Han population. Nat Genet 43(4):345–349
18. Park JW, Cai J, McIntosh I, Jabs EW, Fallin MD, Ingersoll R, Hetmanski JB, Vekemans M, Attie-Bitach T, Lovett M et al (2006) High throughput SNP and expression analyses of candidate genes for non-syndromic oral clefts. J Med Genet 43(7):598–608
19. Bochukova EG, Soneji S, Wall SA, Wilkie AO (2010) Scalp fibroblasts have a shared expression profile in monogenic craniosynostosis. J Med Genet 47(12):803–808
20. Lupu C, Zhu H, Popescu NI, Wren JD, Lupu F (2011) Novel protein ADTRP regulates TFPI expression and function in human endothelial cells in normal conditions and in response to androgen. Blood 118(16):4463–4471
21. Patel MM, Behar AR, Silasi R, Regmi G, Sansam CL, Keshari RS, Lupu F, Lupu C (2018) Role of ADTRP (androgen-dependent tissue factor pathway inhibitor regulating protein) in vascular development and function. J Am Heart Assoc 7(22):e010690
22. Parsons WH, Kolar MJ, Kamat SS, Cognetta AB 3rd, Hulce JJ, Saez E, Kahn BB, Saghatelian A, Cravatt BF (2016) AIG1 and ADTRP are atypical integral membrane hydrolases that degrade bioactive FAHFAs. Nat Chem Biol 12(5):367–372
23. Erikci Ertunc M, Kok BP, Parsons WH, Wang JG, Tan D, Donaldson CJ, Pinto AFM, Vaughan JM, Ngo N, Lum KM et al (2020) AIG1 and ADTRP are endogenous hydrolases of fatty acid esters of hydroxy fatty acids (FAHFAs) in mice. J Biol Chem 295(18):5891–5905
24. Yore MM, Syed I, Moraes-Vieira PM, Zhang T, Herman MA, Homan EA, Patel RT, Lee J, Chen S, Peroni OD et al (2014) Discovery of a class of endogenous mammalian lipids with anti-diabetic and anti-inflammatory effects. Cell 159(2):318–332
25. Klein J, Fasshauer M, Ito M, Lowell BB, Benito M, Kahn CR (1999) beta(3)-adrenergic stimulation differentially inhibits

insulin signaling and decreases insulin-induced glucose uptake in brown adipocytes. J Biol Chem 274(49):34795–34802
26. Cohen P, Levy JD, Zhang Y, Frontini A, Kolodin DP, Svensson KJ, Lo JC, Zeng X, Ye L, Khandekar MJ et al (2014) Ablation of PRDM16 and beige adipose causes metabolic dysfunction and a subcutaneous to visceral fat switch. Cell 156(1–2):304–316
27. Fasshauer M, Klein J, Kriauciunas KM, Ueki K, Benito M, Kahn CR (2001) Essential role of insulin receptor substrate 1 in differentiation of brown adipocytes. Mol Cell Biol 21(1):319–329
28. Sun J, Chen J, Li T, Huang P, Li J, Shen M, Gao M, Sun Y, Liang J, Li X et al (2020) ROS production and mitochondrial dysfunction driven by PU.1-regulated NOX4-p22(phox) activation in Aβ-induced retinal pigment epithelial cell injury. Theranostics 10(25):11637–11655
29. Ikeda K, Kang Q, Yoneshiro T, Camporez JP, Maki H, Homma M, Shinoda K, Chen Y, Lu X, Maretich P et al (2017) UCP1-independent signaling involving SERCA2b-mediated calcium cycling regulates beige fat thermogenesis and systemic glucose homeostasis. Nat Med 23(12):1454–1465
30. Li P, Song R, Yin F, Liu M, Liu H, Ma S, Jia X, Lu X, Zhong Y, Yu L et al (2022) circMRPS35 promotes malignant progression and cisplatin resistance in hepatocellular carcinoma. Mol Ther 30(1):431–447
31. Enerbäck S, Jacobsson A, Simpson EM, Guerra C, Yamashita H, Harper ME, Kozak LP (1997) Mice lacking mitochondrial uncoupling protein are cold-sensitive but not obese. Nature 387(6628):90–94
32. Bukowiecki L, Collet AJ, Follea N, Guay G, Jahjah L (1982) Brown adipose tissue hyperplasia: a fundamental mechanism of adaptation to cold and hyperphagia. Am J Physiol 242(6):E353-359
33. Guerra C, Koza RA, Yamashita H, Walsh K, Kozak LP (1998) Emergence of brown adipocytes in white fat in mice is under genetic control. Effects on body weight and adiposity. J Clin Invest 102(2):412–420
34. Barbatelli G, Murano I, Madsen L, Hao Q, Jimenez M, Kristiansen K, Giacobino JP, De Matteis R, Cinti S (2010) The emergence of cold-induced brown adipocytes in mouse white fat depots is determined predominantly by white to brown adipocyte transdifferentiation. Am J Physiol Endocrinol Metab 298(6):E1244-1253
35. Li K, Feng T, Liu L, Liu H, Huang K, Zhou J (2021) Hepatic proteomic analysis of selenoprotein T Knockout Mice By TMT: implications for the role of selenoprotein T in glucose and lipid metabolism. Int J Mol Sci 22:16
36. de Jesus LA, Carvalho SD, Ribeiro MO, Schneider M, Kim S-W, Harney JW, Larsen PR, Bianco AC (2001) The type 2 iodothyronine deiodinase is essential for adaptive thermogenesis in brown adipose tissue. J Clin Investig 108(9):1379–1385
37. Westerberg R, Mansson JE, Golozoubova V, Shabalina IG, Backlund EC, Tvrdik P, Retterstol K, Capecchi MR, Jacobsson A (2006) ELOVL3 is an important component for early onset of lipid recruitment in brown adipose tissue. J Biol Chem 281(8):4958–4968
38. van de Peppel J, Strini T, Tilburg J, Westerhoff H, van Wijnen AJ, van Leeuwen JP (2017) Identification of three early phases of cell-fate determination during osteogenic and adipogenic differentiation by transcription factor dynamics. Stem Cell Reports 8(4):947–960
39. Velazquez-Villegas LA, Perino A, Lemos V, Zietak M, Nomura M, Pols TWH, Schoonjans K (2018) TGR5 signalling promotes mitochondrial fission and beige remodelling of white adipose tissue. Nat Commun 9(1):245
40. Luck K, Kim DK, Lambourne L, Spirohn K, Begg BE, Bian W, Brignall R, Cafarelli T, Campos-Laborie FJ, Charloteaux B et al (2020) A reference map of the human binary protein interactome. Nature 580(7803):402–408
41. Yu H, Tardivo L, Tam S, Weiner E, Gebreab F, Fan C, Svrzikapa N, Hirozane-Kishikawa T, Rietman E, Yang X et al (2011) Next-generation sequencing to generate interactome datasets. Nat Methods 8(6):478–480
42. Wang J, Huo K, Ma L, Tang L, Li D, Huang X, Yuan Y, Li C, Wang W, Guan W et al (2011) Toward an understanding of the protein interaction network of the human liver. Mol Syst Biol 7:536
43. Kim TH, Jo SH, Choi H, Park JM, Kim MY, Nojima H, Kim JW, Ahn YH (2014) Identification of Creb3l4 as an essential negative regulator of adipogenesis. Cell Death Dis 5:e1527
44. Goncalves CA, Leite MC, Guerra MC (2010) Adipocytes as an important source of serum S100B and possible roles of this protein in adipose tissue. Cardiovasc Psychiatry Neurol 2010:790431
45. Zeng X, Ye M, Resch JM, Jedrychowski MP, Hu B, Lowell BB, Ginty DD, Spiegelman BM (2019) Innervation of thermogenic adipose tissue via a calsyntenin 3beta-S100b axis. Nature 569(7755):229–235
46. Xue H, Wang Z, Hua Y, Ke S, Wang Y, Zhang J, Pan YH, Huang W, Irwin DM, Zhang S (2018) Molecular signatures and functional analysis of beige adipocytes induced from in vivo intra-abdominal adipocytes. Sci Adv 4(7):eaar5319
47. Blondin DP, Nielsen S, Kuipers EN, Severinsen MC, Jensen VH, Miard S, Jespersen NZ, Kooijman S, Boon MR, Fortin M et al (2020) Human brown adipocyte thermogenesis is driven by beta2-AR stimulation. Cell Metab 32(2):287–300
48. Morrison SF (2016) Central neural control of thermoregulation and brown adipose tissue. Autonomic Neurosci Basic Clin 196:14–24
49. Zeng W, Pirzgalska RM, Pereira MM, Kubasova N, Barateiro A, Seixas E, Lu YH, Kozlova A, Voss H, Martins GG et al (2015) Sympathetic neuro-adipose connections mediate leptin-driven lipolysis. Cell 163(1):84–94
50. Kazak L, Chouchani ET, Jedrychowski MP, Erickson BK, Shinoda K, Cohen P, Vetrivelan R, Lu GZ, Laznik-Bogoslavski D, Hasenfuss SC et al (2015) A creatine-driven substrate cycle enhances energy expenditure and thermogenesis in beige fat. Cell 163(3):643–655
51. Chi J, Wu Z, Choi CHJ, Nguyen L, Tegegne S, Ackerman SE, Crane A, Marchildon F, Tessier-Lavigne M, Cohen P (2018) Three-dimensional adipose tissue imaging reveals regional variation in beige fat biogenesis and PRDM16-dependent sympathetic neurite density. Cell Metab 27(1):226-236.e223
52. Bartelt A, Bruns OT, Reimer R, Hohenberg H, Ittrich H, Peldschus K, Kaul MG, Tromsdorf UI, Weller H, Waurisch C et al (2011) Brown adipose tissue activity controls triglyceride clearance. Nat Med 17(2):200–205
53. Luo C, Pook E, Tang B, Zhang W, Li S, Leineweber K, Cheung SH, Chen Q, Bechem M, Hu JS et al (2017) Androgen inhibits key atherosclerotic processes by directly activating ADTRP transcription. Biochim Biophys Acta Mol Basis Dis 1863(9):2319–2332
54. Chinetti-Gbaguidi G, Copin C, Derudas B, Vanhoutte J, Zawadzki C, Jude B, Haulon S, Pattou F, Marx N, Staels B (2015) The coronary artery disease-associated gene C6ORF105 is expressed in human macrophages under the transcriptional control of PPARγ. FEBS Lett 589(4):461–466
55. Ahmadian M, Liu S, Reilly SM, Hah N, Fan W, Yoshihara E, Jha P, De Magalhaes Filho CD, Jacinto S, Gomez AV et al (2018) ERRgamma preserves brown fat innate thermogenic activity. Cell Rep 22(11):2849–2859
56. Fitzgibbons TP, Kogan S, Aouadi M, Hendricks GM, Straubhaar J, Czech MP (2011) Similarity of mouse perivascular and brown

adipose tissues and their resistance to diet-induced inflammation. Am J Physiol Heart Circ Physiol 301(4):H1425-1437
57. Kawahito H, Yamada H, Irie D, Kato T, Akakabe Y, Kishida S, Takata H, Wakana N, Ogata T, Ikeda K et al (2013) Periaortic adipose tissue-specific activation of the renin-angiotensin system contributes to atherosclerosis development in uninephrectomized apoE-/- mice. Am J Physiol Heart Circ Physiol 305(5):H667-675
58. Chang L, Villacorta L, Li R, Hamblin M, Xu W, Dou C, Zhang J, Wu J, Zeng R, Chen YE (2012) Loss of perivascular adipose tissue on peroxisome proliferator-activated receptor-gamma deletion in smooth muscle cells impairs intravascular thermoregulation and enhances atherosclerosis. Circulation 126(9):1067–1078
59. Xiong W, Zhao X, Villacorta L, Rom O, Garcia-Barrio MT, Guo Y, Fan Y, Zhu T, Zhang J, Zeng R et al (2018) Brown adipocyte-specific PPARgamma (peroxisome proliferator-activated receptor gamma) deletion impairs perivascular adipose tissue development and enhances atherosclerosis in mice. Arterioscler Thromb Vasc Biol 38(8):1738–1747